Acta Materialia 276 (2024) 120129

Contents lists available at ScienceDirect

Acta Materialia

journal homepage: www.elsevier.com/locate/actamat

Full length article

Magnetization reversal process in flat and patterned exchange-biased CoO/[Co/Pd] thin films

Marcin Perzanowski [a,*], Juliusz Chojenka [a], Aleksandra Szkudlarek [b], Michal Krupinski [a]

[a] Institute of Nuclear Physics Polish Academy of Sciences, Radzikowskiego 152, Krakow, 31-342, Poland
[b] Academic Centre for Materials and Nanotechnology, AGH University of Science and Technology, Mickiewicza 30, Krakow, 30-059, Poland

ARTICLE INFO

Keywords:
Exchange bias
Magnetic thin films
Nanostructured materials
Magnetization process
Patterning

ABSTRACT

Nanostructured magnetic materials have gained great interest due to their possible technological applications in electronic and spintronic devices or in medicine as drug carriers. The key issue which decides on their potential industrial utilization is an exhibited type of a magnetization reversal process. Two main approaches used to describe the switching mechanism are the domain wall motion and coherent magnetization rotation, known as the Kondorsky and Stoner–Wohlfarth models, respectively. The reversal modes can be distinguished by angular measurements of hysteresis loops; however, in many experimental reports the dependencies do not precisely follow either of the models. This makes the question of how the magnetization reversal takes place and how to control or modify it one of the unclear and worth investigation issues in the research on magnetic materials. In this paper, we present our studies on the magnetization reversal in the exchange-biased CoO/[Co/Pd] thin films deposited on a flat substrate and on an array of anodized titanium oxide nanostructures. We studied the reversal mechanism using hysteresis loops and First-Order Reversal Curves. Interestingly, instead of the typical for the flat Co/Pd multilayers Kondorsky process, the system shows a crossover between the domain wall motion and the coherent rotation. A similar situation takes place for the pattern sample. Here, we connect this unusual behavior with the interface exchange interaction responsible for the exchange bias effect.

1. Introduction

In our paper, we study the magnetization reversal process for an exchange-biased multilayer system. Exchange bias effect is a phenomenon driven by a unidirectional exchange anisotropy which appears at the interface between a ferromagnet and an antiferromagnet [1]. The most prominent feature associated with the bias effect is a shift of a hysteresis loop along the external field axis [2]. Due to this asymmetry, materials exhibiting the effect can find their possible technological application in magnetic read heads [3], racetrack memory devices [4], magnetic sensors, [5] or media for magnetic recording [6]. It was also shown that the exchange bias effect can be fully controlled by the electric current and voltage [7] and applied in voltage-assisted writing media [8]. The other field to facilitate exchange-biased systems is biomedicine where they can be applied as biosensors [9] or as drug carriers [10,11]. Exchange-biased systems are also one of the novel media for fabrication of devices for neurostimulation and are promising replacements for medical electrodes in therapeutic procedures [12]. It was also suggested that the materials for spintronic devices based on antiferromagnets and utilizing the exchange bias effect can be applied in artificial neural networks and used for neuromorphic computing [13,14] or in thermoelectric devices based on the Nernst effect [15].

The research presented in the paper was done on the multilayer system where CoO was used as the antiferromagnet and Co/Pd was the ferromagnetic part of the system. CoO is considered the model instance for investigations of the exchange bias effect [16–18] while the Co/Pd and Co/Pt multilayers are well-known for their large perpendicular magnetic anisotropy [19,20]. Apart from technical utilization in magnetic storage devices, the multilayers are currently studied in the context of ultrafast spin transfer [21], the presence of the Dzyaloshinskii–Moriya interaction [22], and as a candidate for all-optical switching devices [23]. In our work, the CoO/[Co/Pd] system was deposited on a flat Si single crystal as well as on a nanopatterned anodized titanium substrate. Due to a variety of possible shapes and sizes of such materials, which are dependent on the fabrication procedure, anodized metallic templates were introduced as a route to percolated perpendicular recording media [24–27]. Anodized titanium oxide is also a p- or n-type semiconductor, depending on Ti and O vacancies concentration, with an energy gap of approximately 3 eV [28]. The vacancies can be also responsible for weak ferromagnetic properties of TiO_x [29].

* Corresponding author.
E-mail address: marcin.perzanowski@ifj.edu.pl (M. Perzanowski).

https://doi.org/10.1016/j.actamat.2024.120129
Received 23 January 2024; Received in revised form 9 May 2024; Accepted 22 June 2024
Available online 26 June 2024

These aspects make titanium oxide substrates a valuable platform for investigations of magnetically controlled ferromagnet-semiconductor junctions [30,31], photovoltaics and photocatalysis [32–34], devices utilizing magnetotransport effects [35], and exchange-biased materials [36]. Such diversity of possible applications of titanium oxide makes its combination with exchange-biased materials an interesting platform for future experiments and the development of spintronic or catalytic devices.

The key feature to develop high-performance magnetic systems is deeper understanding of the mechanism behind the magnetization reversal process in these materials. Despite the practical importance of the exchange-biased systems, research on the influence of the interfacial exchange interactions between ferromagnetic and antiferromagnetic layers on the switching processes still has plenty of aspects to explore. The goal of our work is to investigate and characterize an interplay between the exchange bias effect and perpendicular magnetic anisotropy, and an impact of a nanopatterning process. To have a broad context for our research, we performed the experiments on the model [Co/Pd] multilayer magnetically coupled to a well-known CoO antiferromagnet. The focus is aimed at the modifications of the magnetization reversal mechanisms induced by the exchange interactions between the components of the system.

The magnetization reversal mechanism is a term which relates to the way how magnetic moments divert their orientation upon external stimuli e.g. magnetic field. Two basic reversal mechanisms are the Kondorsky [37] and Stoner–Wohlfarth [38] models. In the Kondorsky process, the reversal takes place by the nucleation of magnetic domains with magnetization orientation pointing in the opposite direction than the rest of the material. The nucleation of domains is followed by a subsequent movement of their domain wall across the specimen leading to the reorientation of the overall magnetization direction. The Stoner–Wohlfarth mechanism concerns uniformly magnetized particles which rotate their magnetization orientation under the external magnetic field in a coherent manner. Besides these two essential reversal types there are also more complex modes like fanning, curling, or buckling [39–41]. One of the most common yet powerful experimental techniques to study this magnetic behavior is a hysteresis loop measurement. Although a single loop cannot explicitly indicate the type of the reversal process, the identification can be carried out using a series of hysteresis measurements conducted with the external magnetic field applied at various polar angles Θ from the easy axis of magnetization. The domain wall motion is distinguished by a constant increase of coercivity as the orientation of the applied field diverges from the easy axis. In the most common case of the domain wall motion process observed for thin magnetic films, the angular evolution should follow the Kondorsky relation $1/\cos\Theta$. However, experimental data often deviate from such simple relations making the correlation between the angular coercivity dependence and the reversal mechanism present in a magnetic system a debated and unclear issue [42,43]. Interestingly, instead of a typical for flat Co/Pd and Co/Pd multilayers Kondorsky-type coercivity dependence, our CoO/[Co/Pd] system shows a different behavior. An initial angular rise of coercivity associated with the domain wall movement is followed by its decrease as the orientation of the external magnetic field moves closer to the hard magnetization axis. The latter process can be linked to the coherent rotation of the magnetization described by the Stoner–Wohlfarth model. a crossover between the reversal mechanism driven by the domain wall motion and the coherent rotation of the magnetization. Similar angular dependency with a clear maximum at $\Theta \approx 70°$ was also obtained for the nanostructured CoO/[Co/Pd] sample. To gain a deeper insight into the crossover between the two reversal mechanisms, the angle-dependent hysteresis measurements are complemented by First Order Reversal Curve (FORC) investigations. To confirm the two-stage process, the FORCs were measured for $\Theta = 0°$ where the presence of only domain wall motion mechanism was expected, and at $\Theta = 70°$ where the wall movement starts to be overlapped by the coherent rotation. In the paper, we discuss the influence of the exchange interaction on the appearance of such a double-component magnetization reversal mechanism.

2. Experimental

The samples were prepared on flat and patterned substrates by thermal evaporation in ultra-high vacuum chamber under the pressure of 10^{-7} Pa at room temperature. On the bottom of the system, the 2 nm thick Pd buffer layer was deposited as a buffer layer to separate the magnetic multilayer from the substrate. Next, a Co layer with a thickness of 1 nm was evaporated at the rate of 0.5 nm/min. This layer was further oxidized for 10 min in the pure oxygen atmosphere at the pressure of 3×10^2 Pa to obtain an antiferromagnetic cobalt oxide layer. Then, seven repetitions of the Co(0.3 nm)/Pd(0.9 nm) bilayer were deposited as a ferromagnetic part of the composite. To prevent the system from further oxidation the multilayer was covered with 2 nm of Pd. The deposition rates for Co and Pd were 0.3 nm/min and 0.5 nm/min, respectively. The Pd/CoO/$[Co/Pd]_7$/Pd multilayer was deposited simultaneously on two types of substrates — a flat Si(100) single crystal and on a polycrystalline patterned anodized titanium.

The patterned substrate was prepared as follows. First, a titanium foil (thickness of 0.25 mm, purity 99.7%) was chemically polished using a mixture of hydrofluoric acid (HF, 50%), nitric acid (HNO_3, 65%), and deionized water with a ratio of 6:20:74 in volume. The polishing procedure was carried out for 3 min at room temperature. After that, the material was dried in a stream of air. Next, the first anodization was performed in the electrolyte composed of ammonium fluoride (NH_4F, 0,3 wt.%), deionized water (1.0 vol.%) and ethylene glycol for 24 h using a voltage of 30 V. To obtain well-ordered nanostructures, the anodized part of the Ti foil was then removed in an ultrasonic bath and the substrate was subjected to the second 24 h long anodization using the same electrolyte and voltage. The patterning process was finished by removing the anodized TiO_2 volume of the foil in the ultrasonic bath once again. This resulted in the fabrication of the patterned Ti with bowl-shaped nanostructures.

The analysis of the layered structure of the system was done for the flat multilayer by means of X-ray reflectivity technique (XRR), using PANalytical X'Pert Pro diffractometer equipped with X-ray lamp with Cu anode operated at 40 kV and 30 mA. Morphology investigations of the patterned system were performed using scanning electron microscope (SEM) FEI Versa 3D with acceleration voltage of 10 kV in the secondary electron mode.

Magnetic measurements were carried out using Quantum Design MPMS XL SQUID magnetometer. Prior to each hysteresis measurement, the sample was demagnetized at 300 K. Then, to induce the exchange bias effect, +50 kOe magnetic field was applied and the system was cooled down to 10 K with a sweep rate of 3 K/min in the presence of the external field. The hysteresis measurements were carried out at a constant temperature of 10 K in the external magnetic field range ±50 kOe. Similarly, First-Order Reversal Curves (FORC) were investigated at 10 K after field cooling from 300 K in the +50 kOe external field. However, in this case, before starting the measurement the field was switched between +50 kOe and −50 kOe fifteen times to exclude the influence of the training effect associated with the exchange bias effect [44,45]. The FORC investigations were performed as follows — first, the external field was set to +10 kOe to fully saturate the magnetic system. Then, the field was changed to the reversal field H_r and the measurement of the magnetization M as a function of the external field H was started. After reaching initial +10 kOe the measurement was stopped, the external field was changed to the succeeding reversal field, different than the previous one, and next magnetization curve was recorded. The instrumental increment of H and H_r fields was set to 100 Oe. The hysteresis and FORC measurements were carried out for various polar angles Θ between the external field direction and the normal to the surface of a system. The direction perpendicular to the surface was set to 0° as the reference orientation.

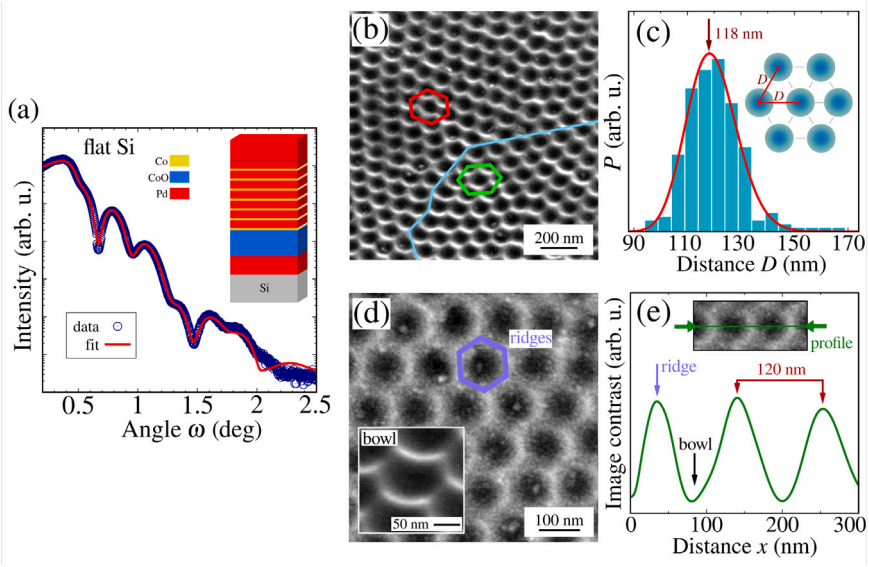

Fig. 1. (a) XRR measurement and the numerical fit for the flat Si(100)/CoO/[Co/Pd] system. (b) SEM image of the CoO/[Co/Pd] system deposited on the patterned Ti substrate. The picture was taken with the electron beam aimed at 45° to the surface normal for better exposure of the nanostructures. Black regions are bowls created by the anodization process. Red and green lines mark different orientations of the patterned hexagonal structures. The blue line indicates the boundary between two structural domains. (c) Distribution of the distances between centers of the nanostructures. The solid line is the log-normal fit. (d) Magnified SEM image of the patterned CoO/[Co/Pd] system. The blue hexagon marks the ridges around a bowl. The inset shows a single bowl-shaped structure. The image was taken with the electron beam aimed at 45° to the surface. (e) Representative cross-section across the nanostructures. (For interpretation of the references to color in this figure legend, the reader is referred to the web version of this article.)

3. Results and discussion

The XRR measurement for the flat Pd/CoO/$[Co/Pd]_7$/Pd sample deposited on the Si(100) substrate (Fig. 1a) confirmed desirable thicknesses of the Co and Pd layers in the $[Co/Pd]_7$ stack and the thicknesses of the buffer and capping Pd layers. The Co layer, which was subjected to the oxidation, had a thickness of 2.5 nm and density of 6.3 g/cm^3. The thickness swallow of this layer is an expected behavior since the oxygen atoms are being incorporated in the Co layer [46,47]. The density of the layer is close to the bulk value of CoO equal to 6.4 g/cm^3 which suggests that this type of cobalt oxide was formed as a result of the oxidation procedure. Therefore, it can be expected that the oxide layer has appropriate antiferromagnetic properties for being magnetically coupled to the ferromagnetic [Co/Pd] stack and to give rise to the exchange bias effect. As both flat and patterned samples were produced in one deposition process with the same growth conditions, the system on the anodized titanium is expected to have an analogous composition to the flat one.

The topography of the CoO/[Co/Pd] system on the patterned Ti was investigated in various places on the sample confirming that the whole surface was uniformly covered with nanostructures and the representative SEM image is shown in Fig. 1b. The anodization process led to the creation of the pattern of hexagonally arranged bowls fabricated in the initial Ti foil. The patterned area is divided into regions within which the hexagonal order of bowls remains unchanged but the overall orientation of a single structural domain is rotated with respect to the neighboring ones. This kind of arrangement is shown in Fig. 1b where the red and green hexagons mark the orientations of the structural domains and the blue line separates two structural regions. The distribution of the distances D between neighboring centers of bowls follows a log-normal function with maximum for 118 nm, as presented in Fig. 1c. Fig. 1d presents a magnified image of the pattern taken within a single structural domain. The picture in the inset was taken with the electron beam aimed at 45° from the surface and shows a single bowl-shaped structure. The bowls are separated from each other by distinct ridges indicated in the picture by the blue hexagon. The ridges are clearly visible in the cross-section taken along nanostructures and presented in Fig. 1e. The vertical distance between a ridge and a bottom of a bowl cannot be precisely determined from SEM images. However, taking into account the shape of the structures observed in the pictures obtained with angled electron beam we can expect that the depth of the bowls is comparable with their radius of approximately 120 nm.

The magnetization reversal mechanism for the CoO/[Co/Pd] multilayers deposited on the flat Si and patterned Ti was studied using a series of hysteresis loops measured at 10 K after cooling in the external magnetic field of +50 kOe. The measurements were carried out for different polar angles Θ between the external field direction and the normal to the surface of a system, and the direction perpendicular to the surface is set to 0°. The orientation of the sample with respect to the external field remained unchanged during the cooling procedure and the following hysteresis or FORC measurement. Before a subsequent measurement for another angle Θ, a sample was heated up to the room temperature and remounted to a new orientation. Exemplary hysteresis loops for both systems are shown in Fig. 2a while corresponding dM/dH switching field distributions, calculated from the loops, are presented in Fig. 2b.

The flat CoO/[Co/Pd] system is single-phase which is reflected in the dM/dH curves by the presence of one symmetrical maximum for each upper and lower magnetization branch. The hysteresis loop measured at $\Theta = 0°$ has a rectangular shape with narrow dM/dH distributions which implies an abrupt magnetization reversal process. The magnetic remanence of the loop at $\Theta = 0°$ is 0.95 of the saturation magnetization and decreases gradually as the Θ angle increases. At the same time, as the angle becomes larger the dM/dH distributions are broader. This indicates that the direction perpendicular to the surface is the easy axis of magnetization which is due to the presence of the Co/Pd multilayer component with strong out of plane magnetic anisotropy. The orientation of the easy axis of magnetization is set as the reference direction $\Theta = 0°$ for further angle-dependent measurements as this direction is referred in the models used for describing the magnetization reversal mechanisms (Kondorsky and Stoner–Wohlfarth).

The values of the coercive field H_c for each polar angle Θ were calculated as $|H_s^+ - H_s^-|/2$ where H_s^+ and H_s^- are dM/dH switching field maxima positions for the upper and lower magnetization branches of a particular hysteresis loop. The angular dependency of H_c for the flat system is displayed in Fig. 2c (upper panel), the data were normalized

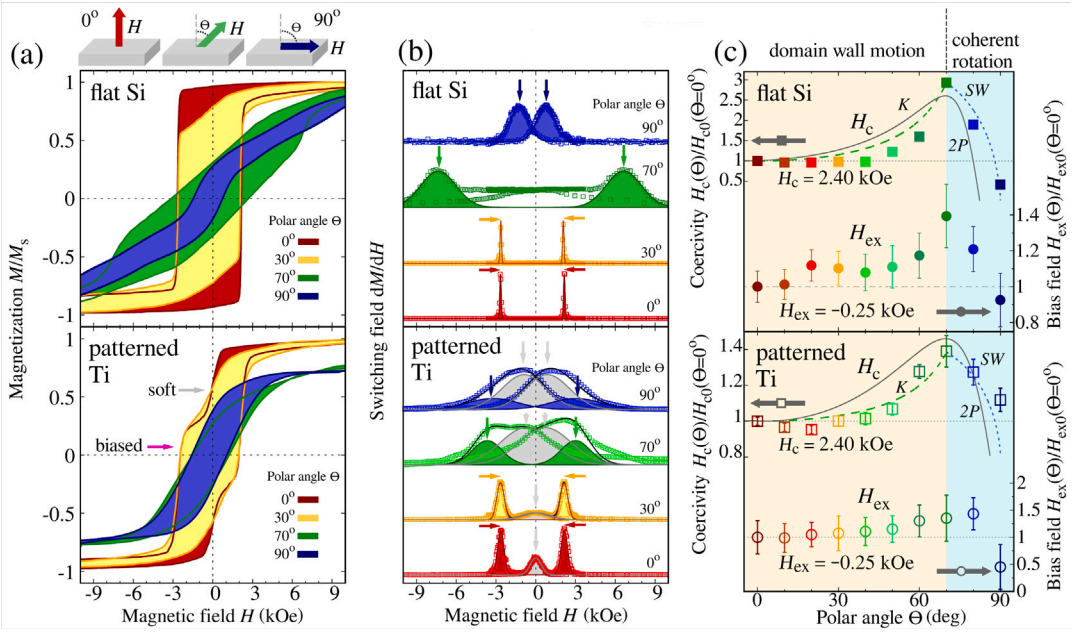

Fig. 2. (a) Exemplary hysteresis loops measured for the CoO/[Co/Pd] system deposited on the flat Si (upper row) and patterned Ti (lower row) substrates. The measurements were done at 10 K after field cooling in +50 kOe for various polar angles Θ between the external field direction and normal to the sample surface. For clarity, the loops are shown only in the ±10 kOe range. The cartoons above the loops schematically show the polar angle Θ. (b) Switching field distributions dM/dH calculated from the hysteresis loops. Experimental data (points) were fitted with Gaussian functions (solid lines). Color areas represent the signals coming from the biased phase. The arrows mark the maxima of the distributions. Gray areas with corresponding arrows indicate the second non-biased magnetic phase observed for the system on the patterned Ti. (c) Angular dependencies of the coercivity field H_c (left scale) and the bias field H_{ex} (right scale) for the systems deposited on flat Si and patterned Ti. The data sets were normalized to the values of coercivity H_{c0} and the bias field H_{ex0} obtained for $\Theta = 0°$ (the reference level 1 is marked in the figure with horizontal dashed lines). Green and blue dashed lines correspond to the Kondorsky (K) relation for the domain wall motion and the Stoner–Wohlfarth (SW) model for the coherent magnetization rotation, respectively. Gray solid lines represent the 2-Phase reversal model ($2P$). The ranges of the angle Θ where the domain wall motion or coherent rotation mechanisms are dominant are marked with orange and blue areas, respectively. Error bars for the H_c and H_{ex} in (c) were calculated using propagation of uncertainty from numerical errors of the fits and taking into account the instrumental step in the vicinity of the dM/dH maximum. (For interpretation of the references to color in this figure legend, the reader is referred to the web version of this article.)

to the value $H_c = 2.4$ kOe obtained for $\Theta = 0°$. In the angle-dependent measurement, coercivity increases gradually to reach its maximum at 70° after which it decreases to a value smaller than for $\Theta = 0°$. The shape of the first part of the dependency is similar to the Kondorsky relation where coercivity is proportional to $1/\cos(\Theta)$ [37] (green dashed line marked as K in Fig. 2c) while the other, above 70°, is analogous to the Stoner–Wohlfarth model (SW, blue dashed line) [38]. Such a result suggests that for low angles Θ the magnetization reversal process is mostly driven by the domain wall motion, and changes to the coherent rotation mode as the direction of the external magnetic field approaches the direction parallel to the film plane. What is worth noting, is that for each loop the magnetization branches are symmetrical in regard to the exchange bias field and reversing the field sweep direction. This suggests that the same magnetization reversal mechanism takes place along the upper and lower magnetization branches.

The initial increase of $H_c(\Theta)$ followed by its steep decline above 70° can be also described using the two-phase model, developed for multidomain crystals [48–50]. In this model, decreasing the external magnetic field below the nucleation field causes the domain walls to appear and move freely in the material. From this point, the system can be considered two-phase. At the same time, the external field also rotates the magnetic moments inside the domains. When the external field approaches negative saturation, the magnetic domains within the material consolidate and the system can be treated as single-phase. This model combines two reversal branches — coherent rotation of magnetization vectors taking place when a system is in the single-phase state, and the domain wall motion following Néel's phase theory [51]. Mathematically, the model is expressed as

$$\frac{H_c^{2P}}{H_{c0}(\Theta)} = 2P = \frac{(N_x + N_N)\cos\Theta}{N_z \sin^2\Theta + (N_x + N_N)\cos^2\Theta} \quad (1)$$

where N_z and $N_x(=N_y)$ are demagnetizing factors associated with the shape anisotropy and $N_N = H_A/M_s$ is the effective demagnetization factor related to the magnetocrystalline anisotropy present in a system. Here, H_A and M_s denote the anisotropy field and saturation magnetization, respectively. It is worth noting that the N_z and N_x are the factors for the direction corresponding to the easy axis of magnetization which, in our case, is perpendicular to the sample surface. Since in the limit of $N_z = 0$ Eq. (1) transforms into typical Kondorsky relation $\propto 1/\cos\Theta$, the presence of a clear maximum in the $H_c(\Theta)$ data indicates that the out-of-plane demagnetization factors are sufficiently large to affect the magnetization reversal mechanism. The two-phase model, applied to the data obtained for the flat CoO/[Co/Pd] multilayer, is shown in Fig. 2c (gray solid line marked as $2P$). Usually, in flat thin films and multilayers, the magnetization switching preferably takes place only by the domain wall motion resulting in the increase of coercivity with angle Θ. Such behavior was shown for Co/Pd and Co/Pt films [24–26,52] as well as for $L1_0$ FePd and FePt [53,54], CoCrPt [55], or Co-Tb alloys [56]. Both of the approaches — the crossover between the Kondorsky and Stoner–Wohlfarth relations and the two-phase model — reproduce the $H_c(\Theta)$ angular results and provide a qualitative picture for describing the magnetization reversal mechanism present in our system.

The hysteresis loops are shifted from zero position towards negative field values which is a sign that the exchange bias effect is present in the samples. The appearance of this shift proves that the oxidized layer of CoO is an antiferromagnet which is exchange coupled to the ferromagnetic Co/Pd multilayer. The exchange bias field H_{ex} was calculated as $|H_s^+ + H_s^-|/2$ using the upper and lower branch dM/dH switching field maxima positions and its angular dependence for the flat film is shown in Fig. 2c (upper panel). The H_{ex} field rises gradually as the direction of the external field deviates from the easy axis of magnetization, reaches a maximum for 70° and then decreases. It is observed that the shape of the $H_{ex}(\Theta)$ and $H_c(\Theta)$ dependencies is qualitatively similar. The ferromagnet–antiferromagnet exchange coupling effectiveness can be

expressed as the H_{ex}/H_c ratio [57]. In this context, a synchronic growth and decline of both H_c and H_{ex} suggests that the coupling strength does not change significantly with the angle at which the external magnetic field is applied during the measurement.

Hysteresis loop measurements with the external magnetic field applied at various polar angles Θ were also performed for the CoO/[Co/Pd] system deposited on the patterned anodized titanium substrate, and the results are depicted in Fig. 2a (lower panel). A distinctive kink observed in the loops, especially pronounced for low Θ angles suggests the presence of two magnetic phases in the patterned system. The appearance of a second magnetic phase is confirmed in the corresponding dM/dH switching field distributions as a set of additional pair of signals (gray areas in Fig. 2b) as compared with the dM/dH distributions for the flat sample. The inner pairs of maxima (marked with gray arrows) display coercivity ranging from several Oe observed for $\Theta=0°$ up to approximately 1 kOe for 90°. Additionally, these maxima show no horizontal loop shift associated with the presence of the exchange bias effect. The appearance of this soft unbiased phase is due to the anodization of the TiO substrate surface which caused increased disorder in the system. Part of the oxidized cobalt did not form the antiferromagnetic oxide and, therefore, did not establish a basis for the magnetic exchange coupling with the ferromagnetic part of the system. Additionally, the jaggedness of the substrate caused the intermixing of Co and Pd atoms and led to softening magnetic properties observed in the initial [Co/Pd] multilayer. A similar effect of altering magnetic properties on the edges of structures upon patterning resulting in the creation of a soft magnetic phase was previously reported in other works [18,36,58–60]. Likewise the loops for the multilayer on the flat Si, the loops recorded for the patterned system are symmetrical around the exchange bias field indicating that a similar switching process takes place for both upper and lower magnetization branches.

The outer high-field pairs of dM/dH maxima (color areas in Fig. 2b, lower panel) observed for each hysteresis loop have larger coercivity than the soft component. Despite the presence of the magnetically soft part of the system originating from the patterning procedure, the hard component shows the coercive and exchange bias fields analogous to those observed for the flat layer. This similarity leads to the conclusion that in both cases of the flat and patterned systems, the same exchange coupling mechanism between CoO and [Co/Pd] is responsible for its appearance. A noticeable difference between hysteresis loops for the flat and patterned systems, especially prominent for low Θ angles, is the broadening of the dM/dH distributions for the system on the anodized Ti. This is due to the curved shape of the substrate which caused larger spatial dispersion of the orientation of the easy axis of magnetization. The angle dependencies of the coercive and bias fields for the pattern sample (Fig. 2c, lower panel) have similar shapes to those observed for the flat system. Therefore, the magnetization reversal can be interpreted as the crossover between domain wall motion observed for low Θ angles and coherent magnetization rotation above Θ = 70°, or, in terms of the two-phase model, by considering a simultaneous existence of both of these mechanisms. However, in comparison the flat film, a significant decrease in the relative peak height $H_c^{max}(\Theta=70°)/H_{c0}(\Theta=0°)$ is observed for the pattern sample. This reduction from 2.9 to 1.4 can be associated with the substrate patterning which made the distribution of the orientation of the easy axis broader, as it is observed in increased dM/dH widths, resulting in the more isotropic magnetic behavior of the system.

Although the simultaneous existence of the domain wall motion and coherent magnetization rotation during the magnetization reversal of a flat thin film is intriguing by itself, the preservation of this behavior for the system deposited on a patterned substrate makes our results even more uncommon. Interestingly, Rahman et al. [25] and Piraux et al. [26] studied Co/Pt films deposited on anodized alumina oxide in the form of holes or bumps and did not report the coercivity angle dependence with the shape observed in our studies. In those cases, the transformation from the initial Kondorsky's domain wall motion model for a flat film to a situation comparable to the Stoner–Wohlfarth coherent rotation in the case of a patterned system was ascribed to the variations of the anisotropy axis orientation. Likewise, Brombacher et al. [55] observed a similar effect for granular CoCrPt-SiO_2 films deposited onto SiO_2 nanoparticles with different sizes. These effects is also present in our results as we discussed the broadening of the dM/dH distributions and decline of the H_c^{max}/H_{c0} ratio for the patterned sample, however, they have a minor influence on the reversal mechanism.

Factor which differs our results from the above-mentioned research concerning magnetization reversal in flat and patterned systems is the presence of the interface exchange interaction between the antiferromagnetic CoO and ferromagnetic [Co/Pd], responsible for the exchange bias effect and the hysteresis loop shift. The appearance of the bias effect is associated to the presence of grains within the antiferromagnet which form domains, as it was postulated in the model formulated by Nowak et al. [61] These domains are created during cooling the antiferromagnet through Néel and blocking temperatures and their appearance is due to structural defects inside a polycrystalline layer [61,62]. An incremental evolution of the domain walls in exchange-coupled ferromagnet/antiferromagnet bilayers was investigated by C. L. Chien et al. [63]. It was shown using magneto-optical indicator film technique that during the magnetization reversal process, domain walls within the ferromagnetic layer relocate, while the domains in the antiferromagnet are motionless. It was also reported that for the case of the FM-AFM interfacial exchange coupling interaction that the domain structure of the antiferromagnet imposes splitting neighboring ferromagnet into domains which are smaller than those which would appear in a purely ferromagnetic system [64]. Additionally, M. Merkel et al. [65,66] investigated antiferromagnetic thin films using Atomic Force Microscopy combined with MOKE magnetometry. They reported on the time-dependent magnetic anisotropies and magnetically effective antiferromagnetic grain size distributions as the key factors influencing the exchange bias effect.

According to these findings, the magnetization reversal process present in our flat system may take place in the following manner. A schematic picture of the reversal mechanism taking place for the angle Θ from 0° to 70° is shown in Fig. 3a. Initially, as the external magnetic field starts to be lower than the saturation field, the nucleation process is initiated. Then, driven by the changes of the external field, the movement of the domain walls develops in accordance with the Kondorsky reversal model. This process is responsible for the increase of the $H_c(\Theta)/H_{c0}$ ratio observed in our results. Above $\Theta=70°$ (Fig. 3b) the coherent magnetization rotation mechanism starts to overshadow the domain wall motion. The domain structure of the antiferromagnet constricts the size of the ferromagnetic domains and prevents further domain wall movement. In this way, the completion of the reversal process as the external field reaches saturation magnetization takes place by the rotation of the magnetization within now static ferromagnetic domains which causes the decrease of the $H_c(\Theta)/H_{c0}$ ratio above 70°. It is also worth pointing out that O'Grady et al. [67] suggested the reversal mechanism of unstable antiferromagnetic grains is similar to Stoner–Wohlfarth coherent magnetization rotation. This may be another factor contributing to the switching mechanism observed in our systems and be partially responsible for the transition from domain wall motion to coherent rotation. The preservation of the $H_c(\Theta)/H_{c0}$ curve shape for the pattern sample suggests that the reversal mechanism present is this system is similar to the hypothesized for the flat multilayer. The influence of the structurization procedure is observed predominantly as dispersion of the easy axis orientation but it does not qualitatively affect the magnetization reversal mechanism.

To acquire a broader overview on the magnetization reversal in our systems, we performed a series of First-Order Reversal Curve (FORC) measurements. The experiments were carried out at 10 K after field cooling the sample under the external field of +50 kOe, large enough to magnetically saturate the material. The measurements were performed

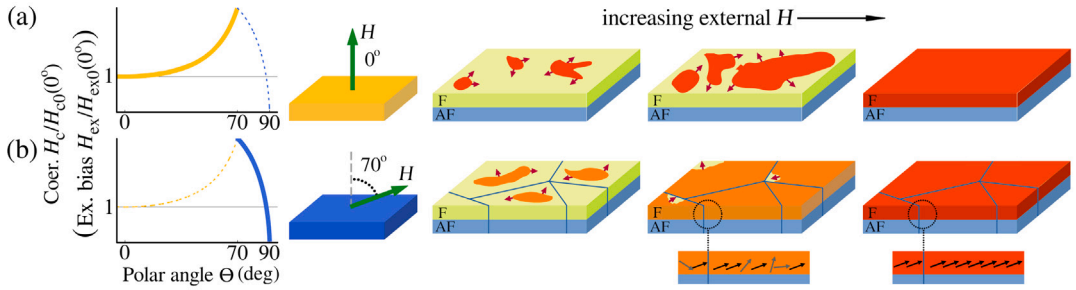

Fig. 3. Schematic depiction of the proposed magnetization reversal mechanisms for the CoO/[Co/Pd] system. (a) Reversal dominated by the domain wall motion for the polar angle Θ from 0° to 70° and (b) for $\Theta > 70°$ where the coherent rotation starts to play an important role in magnetization switching. F and AF denote ferromagnetic and antiferromagnetic components of the system, respectively.

with the external field applied at 0° (out of plane geometry), and at 70° to investigate the reversal mechanism when the $H_c(\Theta)/H_{c0}$ ratio reaches its maximum value. The families of magnetization curves, dependent on the external field H and the reversal field H_r, obtained for the flat and patterned CoO/[Co/Pd] systems are presented in Fig. 4 (first column). The $M(H, H_r)$ curves were recalculated into FORC distributions $\rho(H, H_r)$ using second-order mixed derivative [68]

$$\rho(H, H_r) = -\frac{1}{2}\frac{d^2 M}{\partial H \partial H_r} \tag{2}$$

and the results are shown in the middle column of Fig. 4. In such representation, any nonzero signal is associated with an irreversible magnetization switching, eliminating reversible components for $\rho = 0$. The FORC distribution is also given in the h_c-h_u coordination system (Fig. 4, right column) defined by

$$h_c = \frac{H - H_r}{2}, \qquad h_u = \frac{H + H_r}{2}. \tag{3}$$

In this case, h_c describes the local coercive field of each hysteron, while h_u is the local interaction field which moves the hysteron's center from its zero position [69].

The hysteresis loop for the flat CoO/[Co/Pd] multilayer measured for Θ = 0° shows the steep transition between positive and negative magnetization which is mirrored in the narrow dM/dH distributions (see Fig. 2). This result is typical for a multilayer with strong out of plane magnetic anisotropy and indicates an abrupt magnetization switching. In the FORC results (Fig. 4a–c), this process is reflected by the pair of signals centered around H and H_r fields corresponding to lower and upper switching field maxima H_s^- and H_s^+ observed in the hysteresis loops. The presence of the positive–negative pair can be associated with the magnetization reversal taking place by the nucleation of reversed magnetic domains followed by the subsequent domain wall motion and their final annihilation. Both of the FORC features are narrow indicating a rapid switching process which is consistent with the observations from the hysteresis loop measurement. In the h_c domain, the positive–negative pair is centered around −2.4 kOe which corresponds to the switching field maximum for the lower hysteresis branch H_s^-. The center of the negative FORC signal is shifted by −0.2 kOe along the h_u axis (blue arrow in Fig. 4c) which indicates the presence of the exchange interaction in the system. The value stays in agreement with the exchange bias field found in the corresponding hysteresis loop.

The FORC results obtained for the flat sample with the external field applied at 70° (Fig. 4d–f) are more complex than in the out of plane case. The irreversible magnetization switching process ($\rho(H, H_r) \neq 0$) starts for the external field H of approximately −0.4 kOe and the reversal field H_r of 6 kOe, and ends after H and H_r reach −5.5 kOe and 3.6 kOe, respectively. Within this relatively large range, two remarkable regions can be distinguished — the low-field spot for $H \in$ (−0.4 kOe; −1.8 kOe) and $H_r \in$ (3.6 kOe; 5.3 kOe) (marked as (1) in Fig. 4d–f), and the high-field spot for $H \in$ (−3 kOe;−5.5 kOe) and $H_r \in$ (3.6 kOe; 6 kOe) (spot (2) in Fig. 4d–f). Both regions are interconnected by the negative horizontal ridge centered around the reversal field H_r equal to the positive switching field H_s^+. The high-field spot can be associated with the irreversible magnetization reversal taking place in the vicinity of the switching field maximum H_s^-. It is worth pointing out that the low-field region has no direct counterpart in any evident feature observed in the $M(H)$ or dM/dH curves. The contrast of the positive–negative signal is stronger for the high-field spot than for the low-field region which suggests that the reversal mainly takes place near the H_c. The presence of two separated stages of reversal for $\Theta = 70°$ is in agreement with the angular measurements showing the crossover between the domain wall motion and coherent rotation processes appearing around this angle. These two-stage process is also reflected in the h_c-h_u coordination system where the low-field component is observed for h_c of approximately 2.5 kOe and h_u of 1.5 kOe and the high-field element for h_c and h_u around 4.5 kOe and 0, respectively. The ρ minimum in the FORC signal near the coercive field is shifted towards lower h_u value than in the previous case (Fig. 4c and f) which is compatible with the increase of the bias field and coercivity in the angular measurements (see Fig. 2).

A similar result, where the dM/dH distribution obtained from a hysteresis loop branch has only one maximum while the FORC measurement shows two reversal components, were reported by Miyazawa et al. [70]. The authors associated the low-field FORC spot with the reversal of a multidomain structure while the appearance of the high-field region was assigned to the switching of single-domain objects. Complementary studies were presented by Roberts et al. [71] and Xu et al. [72] where the subject of the multidomain and (pseudo)single-domain influence on FORC distributions was discussed. Following this line of reasoning, the low-field spot in our results may be assigned to the domain wall motion mechanism observed in the angle-dependent results (Fig. 2) originating from the multidomain structure of the ferromagnet. Accordingly, the high-field signal can be correlated with (pseudo)single domain ferromagnetic objects which reverse their magnetization by the coherent rotation. Their presence in the system may be caused by a split of the ferromagnetic layer into small domains whose size is extorted by the domain structure of the antiferromagnet. In the course of the magnetization reversal process, some ferromagnetic parts of the system remained unswitched due to their strong exchange coupling to the antiferromagnet. When the external field become sufficiently high, they coherently reversed their magnetization giving a characteristic fingerprint in the angular H_c measurements and providing additional FORC signal.

The FORC result obtained for the patterned system at angle Θ = 0° (Fig. 4g–i) is qualitatively similar to that measured for the flat multilayer. A single irreversible spot contains a positive–negative signal centered around the external field equal to the negative switching field H_s^-. This suggests that the magnetization reversal mechanism for the external field applied in the out of plane direction is analogous in both cases of the flat and patterned systems. In comparison to the $\rho(H, H_r)$ distribution for the flat sample (Fig. 4b and h), for the patterned system

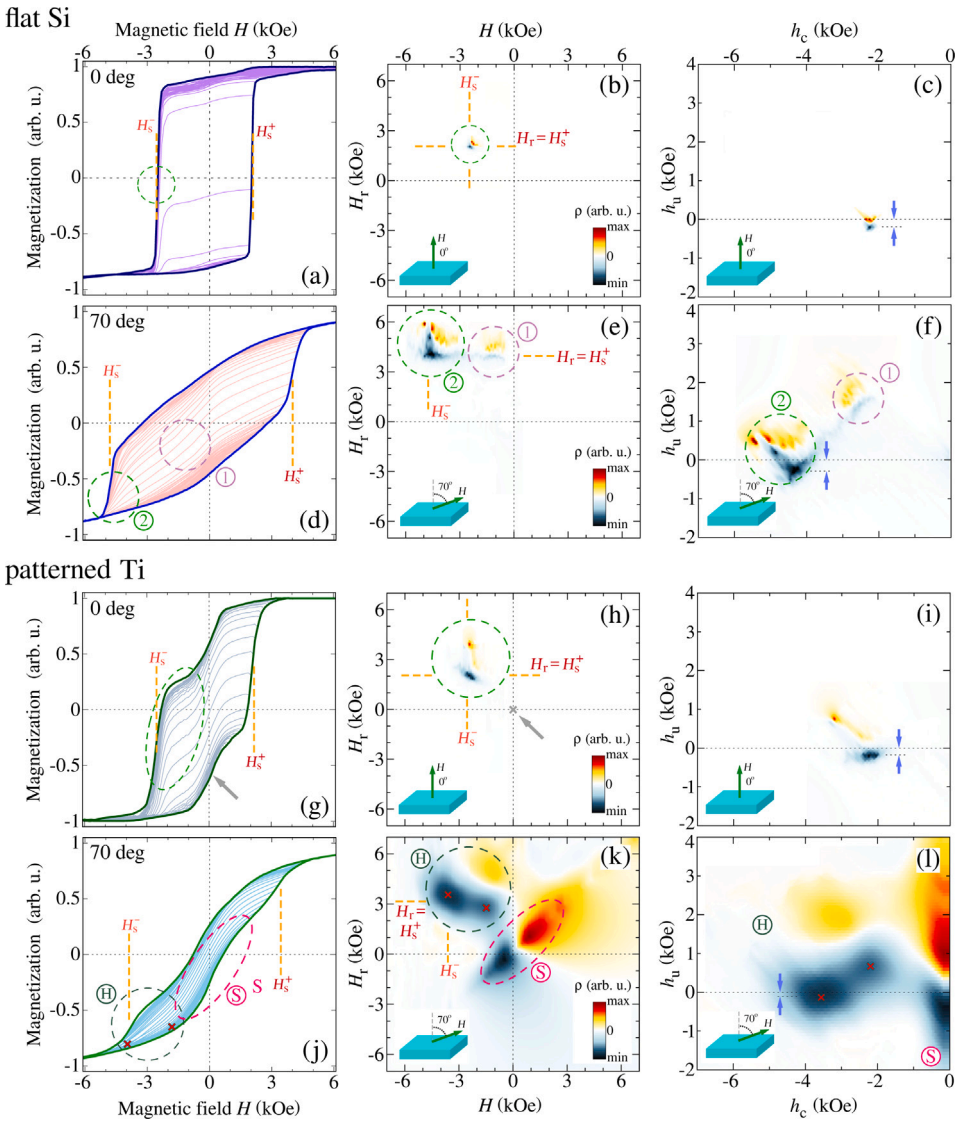

Fig. 4. FORC measurements for the CoO/[Co/Pd] system deposited on the flat Si (upper two rows) and patterned Ti (lower two rows) substrates obtained with the external magnetic field applied at angle $\Theta = 0°$ and 70°. The first column presents the families of FORC curves within the hysteresis loops measured before the FORC studies. The $\rho(H, H_r)$ distributions are given in the second column while the third column shows the ρ distributions in the h_c-h_u coordination system. Dotted red lines mark the positions of the upper H_s^+ and lower H_s^- switching field maxima obtained from the hysteresis loops. Color ovals mark corresponding regions with irreversible magnetization switching. (For interpretation of the references to color in this figure legend, the reader is referred to the web version of this article.)

the positive and negative signals are distinctly spread apart along the vertical H_r axis. The negative spot is located right below the $H_r = H_s^+$ line, similar to the flat sample, while the positive signal appears for larger H_r values. This signifies that the creation of reversed domains takes place at an earlier stage of reversal. The effect is complementary to the broader dM/dH switching field distributions observed in this system and is related to the dispersion of the easy axis orientation arising from the patterning procedure. The negative signal in the h_c-h_u coordination system (Fig. 4i) is shifted below $h_u = 0$ line for approximately the same amount as the signal for the flat sample. This stays in agreement with the angular H_c measurements and the FORC measurements described yet. It is also worth noting that the central signal in the hysteresis loop (H close to zero, gray arrow in Fig. 4g), observed as the inner maxima in the dM/dH distribution (see Fig. 2b), does not give an irreversible signal in the FORC (arrow in Fig. 4h). The lack of this feature in the FORC measurement may be due to the instrumental step in the H and H_r fields during the measurement which is too large to mirror the properties of the weak ferromagnetic material in the ρ distribution.

In the FORC measured for the patterned system at the angle 70° (Fig. 4j–l) the signal coming from the soft phase (marked as S in the figure) is visible as the pair of minimum and maximum of ρ in the H-H_r coordination system (Fig. 4k). Its explicit appearance is related to the apparent ferromagnetic behavior revealed by the soft phase and observed as the coercive field in the hysteresis loop (see Fig. 2). This signal is mirrored in the h_c-h_u plot (Fig. 4l) as the positive–negative pair centered around the $h_c = 0$ line. The vertical shift of this pair with respect to the $h_u = 0$ level suggests that there is a local interaction field which causes the move of hysterons center from the reference zero position. However, due to the lack of the horizontal hysteresis loop shift observed in the measurements (Fig. 2) this effect cannot be directly associated with the presence of the exchange bias effect within the soft phase. The FORC signal recorded for the hard exchange-biased phase (marked as H in the figure) is less pronounced and blurred than its counterpart measured at 70° for the flat system which can be associated with nanostructurization of the system which causes broadening the distribution of orientation of the easy axis of magnetization. While the maximum of ρ is in a form of a plateau, there are two separated FORC minima (red crosses in Fig. 4j–l) observed

for nearly the same H_r value, but separated along the H axis. Such situation is similar to the flat system measured at 70° and suggest the presence of two magnetization components responsible for the two-step magnetization reversal process. As previously, the low-field signal can be associated with the domain wall motion component of the reversal while the high-field spot is linked to coherent rotation of (pseudo)single domain ferromagnetic objects. The vertical shift of the ρ minimum of the high-field spot in the h_c-h_u coordination system (Fig. 4l) is difficult to determine due to blurring of the signal. However, it is located below the $h_u = 0$ line which agrees with the previous results and indicates the presence of the ferromagnet–antiferromagnet exchange interaction in the system.

The angle-dependent hysteresis and FORC results are qualitatively comparable and show the presence of the two-step magnetization reversal mechanism which suggests that the process in both flat and patterned exchange-biased CoO/[Co/Pd] multilayers is similar. When the external magnetic field is applied along the easy axis of magnetization the system switches its magnetization through the domain wall motion. For increasing deviation of the external field direction from the easy axis, the influence of the coherent magnetization rotation becomes progressively compelling up to 70° where it starts to dominate over the wall motion. Interestingly, the patterning procedure resulting in the creation of periodically arranged bowl-shape nanostructures does not change the switching process significantly as it was observed for thin films without the exchange bias effect. Additionally, it is observed that the patterned system consists of two magnetic phases — the biased hard phase, and the softer component without the exchange bias effect. The presence of the second phase was observed in the hysteresis loops as well as in the FORC result. However, despite its appearance the angular dependencies of H_c and H_{ex} and the FORC distributions for the hard phase are similar for the flat and patterned systems. This indicates the influence of the soft phase on the reversal of the biased component is minor or negligible. As it was indicated in other works, domains in the antiferromagnet are motionless while the ferromagnet switches its magnetization orientation. In our case, the orientation of the domains within the CoO layer was extorted by the external field during the cooling procedure. The exchange interaction of these frozen domains with the ferromagnetic part of the systems determined the way in which the magnetization reversal took place. This points to the exchange bias effect as the main driving force dominating the reversal and overshadowing other factors such as the influence of the nanopatterned surface or the presence of the second non-biased magnetic phase in the system.

4. Conclusions

In this paper, we studied the magnetization reversal mechanism of the exchange-biased CoO/[Co/Pd] multilayer with the out of plane magnetic anisotropy deposited on the flat and patterned substrates. The research was conducted using angle-dependent hysteresis loop measurements and first order reversal curve technique. Typically, for flat ferromagnetic thin films, including Co/Pd and Co/Pt systems, the reversal takes place through the domain wall motion while the coherent magnetization rotation process is more common for assemblies of nanoparticles. The most important factor that distinguishes our research is the presence of the magnetic exchange interaction between the ferromagnetic Co/Pd and antiferromagnetic CoO leading to the appearance of the exchange bias effect. This also led to an alteration of the magnetization reversal and caused the mechanism to be the crossover between the domain wall motion and the coherent rotation which was observed in the angle-dependent hysteresis measurements as the gradual increase of coercivity followed by its steep decline. The existence of the two-stage process was also confirmed by the First-Order Reversal Curve studies where we observed a single reversal region with the external field applied out of plane and two separated reversal processes when the field was directed at 70° from the normal to the surface. Such magnetic behavior may be assigned to the domain structure of the ferromagnet influenced and arranged by the static domains in the antiferromagnet. The characteristic two-stage process was observed for the flat film and preserved for the system deposited on the patterned substrate. The main contribution of the patterning procedure was the spatial broadening of the easy axis orientation distribution.

CRediT authorship contribution statement

Marcin Perzanowski: Conceptualization, Formal analysis, Investigation, Writing – original draft, Writing – review & editing. **Juliusz Chojenka:** Investigation, Methodology, Validation. **Aleksandra Szkudlarek:** Investigation, Methodology, Validation. **Michal Krupinski:** Methodology, Project administration, Supervision, Validation, Writing – review & editing.

Declaration of competing interest

The authors declare that they have no known competing financial interests or personal relationships that could have appeared to influence the work reported in this paper.

References

[1] M. Kiwi, Exchange bias theory, J. Magn. Magn. Mater. 234 (2001) 584–595.
[2] T. Blachowicz, A. Ehrmann, Exchange bias in thin films — An update, Coatings 11 (2021) 122.
[3] S. Parkin, X. Jiang, C. Kaiser, A. Panchula, K. Roche, M. Samant, Magnetically engineered spintronic sensors and memory, Proc. IEEE 91 (2003) 661–679.
[4] I. Polenciuc, A.J. Vick, D.A. Allwood, T.J. Hayward, G. Vallejo-Fernandez, K. O'Grady, A. Hirohata, Domain wall pinning for racetrack memory using exchange bias, Appl. Phys. Lett. 105 (2014) 162406.
[5] B. Negulescu, D. Lacour, F. Montaigne, A. Gerken, J. Paul, V. Spetter, J. Marien, D. Duret, M. Hehn, Wide range and tunable linear magnetic tunnel junction sensor using two exchange pinned electrodes, Appl. Phys. Lett. 95 (2009) 112502.
[6] D. Suess, T. Schrefl, S. Fähler, M. Kirschner, G. Hrkac, F. Dorfbauer, J. Fidler, Exchange spring media for perpendicular recording, Appl. Phys. Lett. 87 (2005) 112502.
[7] L. Wei, Z. Hu, G. Du, Y. Yuan, J. Wang, H. Tu, B. You, S. Zhou, J. Qu, H. Liu, R. Zheng, Y. Hu, J. Du, Full electric control of exchange bias at room temperature by resistive switching, Adv. Mater. 30 (2018) 1801885.
[8] M. Huang, M.U. Hasan, K. Klyukin, D. Zhang, D. Lyu, P. Gargiani, M. Valvidares, S. Sheffels, A. Churikova, F. Büttner, J. Zehner, L. Caretta, K.Y. Lee, J. Chang, J.P. Wang, K. Leistner, B. Yildiz, G.S.D. Beach, Voltage control of ferrimagnetic order and voltage-assisted writing of ferrimagnetic spin textures, Nat. Nanotechnol. 16 (2021) 981–988.
[9] A. Ehresmann, I. Koch, D. Holzinger, Manipulation of superparamagnetic beads on patterned exchange-bias layer systems for biosensing applications, Sensors 15 (2015) 28854–28888.
[10] M.T. Klem, D.A. Resnick, K. Gilmore, M. Young, Y.U. Idzerda, T. Douglas, Synthetic control over magnetic moment and exchange bias in all-oxide materials encapsulated within a spherical protein cage, J. Am. Chem. Soc. 129 (2007) 197–201.
[11] B. Issa, I.M. Obaidat, B.A. Albiss, Y. Haik, Magnetic nanoparticles: Surface effects and properties related to biomedicine applications, Int. J. Mol. Sci. 14 (2013) 21266–21305.
[12] R. Saha, K. Wu, R.P. Bloom, S. Liang, D. Tonini, J.P. Wang, A review on magnetic and spintronic neurostimulation: Challenges and prospects, Nanotechnology 33 (2022) 182004.
[13] J. Kang, J. Ryu, J.G. Choi, T. Lee, J. Park, S. Lee, H. Jang, Y.S. Jung, K.J. Kim, B.G. Park, Current-induced manipulation of exchange bias in IrMn/NiFe bilayer structures, Nature Commun. 12 (2021) 6420.
[14] S. Fukami, H. Ohno, Perspective: Spintronic synapse for artificial neural network, J. Appl. Phys. 124 (2018) 151904.
[15] H. Zhang, J. Koo, C. Xu, M. Sretenovic, B. Yan, X. Ke, Exchange-biased topological transverse thermoelectric effects in a Kagome ferrimagnet, Nature Commun. 13 (2022) 1091.
[16] E. Menéndez, H. Modarresi, T. Dias, J. Geshev, L.M.C. Pereira, K. Temst, A. Vantomme, Tuning the ferromagnetic-antiferromagnetic interfaces of granular Co-CoO exchange bias systems by annealing, J. Appl. Phys. 115 (2014) 133915.
[17] A.N. Dobrynin, D. Givord, Exchange bias in a Co/CoO/Co trilayer with two different ferromagnetic-antiferromagnetic interfaces, Phys. Rev. B 85 (2012) 014413.

[18] M. Perzanowski, O. Polit, J. Chojenka, W. Sas, A. Zarzycki, M. Marszalek, Magnetic anisotropy in the exchange-biased laser-patterned thin Co/CoO films, Nanotechnology 33 (2022) 495707.

[19] P.F. Carcia, A.D. Meinhaldt, A. Suna, Perpendicular magnetic anisotropy in Pd/Co thin film layered structures, Appl. Phys. Lett. 47 (1985) 178–180.

[20] M.T. Rahman, R.K. Dumas, N. Eibagi, N.N. Shams, Y.-C. Wu, K. Liu, C.-H. Lai, Controlling magnetization reversal in Co/Pt nanostructures with perpendicular anisotropy, Appl. Phys. Lett. 94 (2009) 042507.

[21] Q. Remy, J. Hohlfeld, M. Vergès, Y. Le Guen, J. Gorchon, G. Malinowski, S. Mangin, M. Hehn, Accelerating ultrafast magnetization reversal by non-local spin transfer, Nature Commun. 14 (2023) 445.

[22] E. Pandey, B. Ojha, S. Bedanta, Emergence of sizeable interfacial Dzyaloshinskii-Moriya interaction at cobalt/fullerene interface, Phys. Rev. A 19 (2023) 044013.

[23] N.W.G. Smith, Y. Pleimling, B.A. Magill, R.R.H.H. Mudiyanselage, A. Shenenberger, S. Ogawa, N. Nishizawa, H. Munekata, G.A. Khodaparast, Probe and control of photo-excited magnetization precession in Co/Pd multilayer films at low laser fluence regime, J. Appl. Phys. 132 (2022) 243902.

[24] C. Schulze, M. Faustini, J. Lee, H. Schletter, M.U. Lutz, P. Krone, M. Gass, K. Sader, A. Bleloch, M. Hietschold, M. Fuger, D. Suess, J. Fidler, U. Wolff, V. Neu, D. Grosso, D. Makarov, M. Albrecht, Magnetic films on nanoperforated templates: A route towards percolated perpendicular media, Nanotechnology 21 (2010) 495701.

[25] M.T. Rahman, N.N. Shams, C.H. Lai, J. Fidler, D. Suess, Co/Pt perpendicular antidot arrays with engineered feature size and magnetic properties fabricated on anodic aluminum oxide templates, Phys. Rev. B 81 (2010) 14418.

[26] L. Piraux, V.A. Antohe, F. Abreu Araujo, S.K. Srivastava, M. Hehn, D. Lacour, S. Mangin, T. Hauet, Periodic arrays of magnetic nanostructures by depositing Co/Pt multilayers on the barrier layer of ordered anodic alumina templates, Appl. Phys. Lett. 101 (2012) 013110.

[27] M. Krupinski, M. Perzanowski, A. Maximenko, Y. Zabila, M. Marszalek, Fabrication of flexible highly ordered porous alumina templates by combined nanosphere lithography and anodization, Nanotechnology 28 (2017) 194003.

[28] J. Nowotny, T. Bak, M.K. Nowotny, L.R. Sheppard, Titanium dioxide for solar-hydrogen II. Defect chemistry, Int. J. Hydrog. Energy 32 (2007) 2630–2643.

[29] X. Wei, R. Skomski, B. Balamurugan, Z.G. Sun, S. Ducharme, D.J. Sellmyer, Magnetism of TiO and TiO_2 nanoclusters, J. Appl. Phys. 105 (2009) C51707.

[30] J. Chojenka, A. Zarzycki, M. Perzanowski, M. Krupinski, T. Fodor, K. Vad, M. Marszalek, Tuning of the titanium oxide surface to control magnetic properties of thin iron films, Materials 16 (2023) 289.

[31] J. Chojenka, A. Zarzycki, M. Perzanowski, T. Fodor, K. Mróz, V. Takáts, K. Vad, M. Krupinski, M. Marszałek, Manipulating electrical properties of nanopatterned double-barrier schottky junctions in Ti/TiO_x/Fe systems, J. Phys. Chem. C 128 (2024) 364–374.

[32] T.T. Guaraldo, J.F. de Brito, D. Wood, M.V.B.A. Zanoni, New Si/TiO_2/Pt p–n junction semiconductor to demonstrate photoelectrochemical CO_2 conversion, Electrochim. Acta 185 (2015) 117–124.

[33] M. Humayun, F. Raziq, A. Khan, W. Luo, Modification strategies of TiO_2 for potential applications in photocatalysis: A critical review, Green Chem. Lett. Rev. 11 (2018) 86–102.

[34] M.G. Méndez-Medrano, E. Kowalska, A. Lehoux, A. Herissan, B. Ohtani, S. Rau, C. Colbeau-Justin, J.L. Rodríguez-López, H. Remita, Surface modification of TiO_2 with Au nanoclusters for efficient water treatment and hydrogen generation under visible light, J. Phys. Chem. C 120 (2016) 25010–25022.

[35] A. Zarzycki, J. Chojenka, M. Perzanowski, M. Marszalek, Electrical transport and magnetic properties of metal/metal oxide/metal junctions based on anodized metal oxides, Materials 14 (2021) 2390.

[36] W.-B. Wu, J. Kasiuk, T.N.A. Nguyen, J. Przewoźnik, J. Fedotova, C. Kapusta, O. Kupreeva, S. Lazarouk, K.T. Do, T.H. Nguyen, H.K. Vu, H.L. Pham, D.L. Vu, J. Akerman, Influence of interfacial magnetic ordering and field-cooling effect on perpendicular exchange bias and magnetoresistance in nanoporous IrMn/[Co/Pd] films, J. Appl. Phys. 127 (2020) 223904.

[37] E. Kondorsky, On hysteresis in ferromagnetics, J. Phys. 2 (1940) 161.

[38] E.C. Stoner, E.P. Wohlfarth, A mechanism of magnetic hysteresis in heterogeneous alloys, Phil. Trans. R. Soc. A 240 (1948) 599, reprinted in IEEE Trans. Magn. 27 (1991) 3475–3518.

[39] J. Escrig, M. Daub, P. Landeros, K. Nielsch, D. Altbir, Angular dependence of coercivity in magnetic nanotubes, Nanotechnology 18 (2007) 445706.

[40] W.F. Brown Jr., Criterion for uniform micromagnetization, Phys. Rev. 105 (1957) 1479.

[41] A. Aharoni, First approximation to magnetization curling in a chain of spheres, J. Appl. Phys. 35 (1964) 347–349.

[42] H. Hayasaka, M. Nishino, S. Miyashita, Microscopic study on the angular dependence of coercivity at zero and finite temperatures, Phys. Rev. B 105 (2022) 224414.

[43] J. Li, H. Sepehri-Amin, T. Ohkubo, K. Hono, Identifying the mechanism of hard magnet coercivity by its angular dependence, Phys. Rev. B 105 (2022) 174432.

[44] M. Perzanowski, A. Zarzycki, J. Gregor-Pawlowski, M. Marszalek, Magnetization reversal mechanism in exchange-biased spring-like thin-film composite, ACS Appl. Mater. Int. 12 (2020) 39926–39934.

[45] C. Binek, Training of the exchange-bias effect: A simple analytic approach, Phys. Rev. B 70 (2004) 014421.

[46] M. Perzanowski, M. Marszalek, A. Zarzycki, M. Krupinski, A. Dziedzic, Y. Zabila, Influence of superparamagnetism on exchange anisotropy at CoO/[Co/Pd] interfaces, ACS Appl. Mater. Interfaces 8 (2016) 28159–28165.

[47] O. Hellwig, S. Maat, J.B. Kortright, E.E. Fullerton, Magnetic reversal of perpendicularly-biased Co/Pt multilayers, Phys. Rev. B 65 (2002) 144418.

[48] A. Urzhumtsev, V. Maltseva, A. Volegov, Magnetization reversal processes in sintered permanent magnets $Sm(Co, Fe, Zr, Cu)_Z$, J. Magn. Magn. Mater. 551 (2022) 169143.

[49] M. Mathews, E.P. Houwman, H. Boschker, G. Rijnders, D.H.A. Blank, Magnetization reversal mechanism in $La_{0.67}Sr_{0.33}MnO_3$ thin films on $NdGaO_3$ substrates, J. Appl. Phys. 107 (2010) 013904.

[50] A. Zarzycki, M. Perzanowski, M. Krupinski, M. Marszalek, Solid-state dewetting as a driving force for structural transformation and magnetization reversal mechanism in FePd thin films, Materials 16 (2023) 92.

[51] L. Néel, R. Pauthenet, G. Rimet, V.S. Giron, On the laws of magnetization of ferromagnetic single crystals and polycrystals. Application to uniaxial compounds, J. Appl. Phys. 31 (1960) S27.

[52] Y.T. Yang, J. Li, X.L. Peng, B. Hong, X.Q. Wang, H.L. Ge, Electrical modulation of magnetism in multiferroic heterostructures at room temperature, J. Mater. Sci. 52 (2017) 3330–3336.

[53] M. Perzanowski, M. Krupinski, A. Zarzycki, Y. Zabila, M. Marszalek, Structural ordering of laser-processed FePdCu thin alloy films, J. Alloy. Compd. 646 (2015) 773–779.

[54] J.Y. Shi, X.F. Hu, M. Tang, J. Xu, L.Q. Shen, S.M. Zhou, X.J. Yang, Y.Z. Wu, L.Y. Chen, H.B. Zhao, Ultrafast laser induced magnetization reversal in $L1_0$ FePt films with different chemical orders, AIP Adv. 9 (2019) 035039.

[55] C. Brombacher, M. Falke, F. Springer, H. Rohrmann, A. Goncharov, T. Schrefl, A. Bleloch, M. Albrecht, Magnetic hedgehog-like nanostructures, Appl. Phys. Lett. 97 (2010) 102508.

[56] R. Hussain, B. Aakansha Brahma, R.K. Basumatary, R. Brahma, S. Ravi, S.K. Srivastava, Sperimagnetism in perpendicularly magnetized Co-Tb alloy-based thin films, J. Supercond. Nov. Magn. 32 (2019) 4027–4031.

[57] D.-H. Han, J.-G. Zhu, J.H. Judy, NiFe/NiO bilayers with high exchange coupling and low coercive fields, J. Appl. Phys. 81 (1997) 4996–4998.

[58] C. Castán-Guerrero, J. Herrero-Albillos, J. Bartolomé, F. Bartolomé, L.A. Rodríguez, C. Magén, F. Kronast, P. Gawronski, O. Chubykalo-Fesenko, K.J. Merazzo, P. Vavassori, P. Strichovanec, J. Sesé, L.M. García, Magnetic antidot to dot crossover in Co and Py nanopatterned thin films, Phys. Rev. B 89 (2014) 144405.

[59] M. Perzanowski, M. Krupinski, A. Zarzycki, A. Dziedzic, Y. Zabila, M. Marszalek, Exchange bias in the $[CoO/Co/Pd]_{10}$ antidot large area arrays, ACS Appl. Mater. Interfaces 9 (2017) 33250–33256.

[60] J.M. Shaw, S.E. Russek, T. Thomson, M.J. Donahue, B.D. Terris, O. Hellwig, E. Dobisz, M.L. Schneider, Reversal mechanisms in perpendicularly magnetized nanostructures, Phys. Rev. B 78 (2008) 024414.

[61] U. Nowak, K.D. Usadel, J. Keller, P. Miltényi, B. Beschoten, G. Güntherodt, Domain state model for exchange bias. I. Theory, Phys. Rev. B 66 (2002) 014430.

[62] J. Moritz, P. Bacher, B. Dieny, Magnetic domain wall coercivity and aftereffect in antiferromagnetic/ferromagnetic bilayers, Phys. Rev. B 90 (2014) 024429.

[63] C.L. Chien, V.S. Gornakov, V.I. Nikitenko, A.J. Shapiro, R.D. Shull, Hybrid domain walls and antiferromagnetic domains in exchange-coupled ferromagnet/antiferromagnet bilayers, Phys. Rev. B 68 (2003) 014418.

[64] A. Harres, J. Geshev, A polycrystalline model for magnetic exchange bias, J. Phys.: Condens. Matter. 24 (2012) 326004.

[65] M. Merkel, R. Huhnstock, M. Reginka, D. Holzinger, M. Vogel, A. Ehresmann, J. Zehner, K. Leistner, Interrelation between polycrystalline structure and time-dependent magnetic anisotropies in exchange-biased bilayers, Phys. Rev B. 102 (2020) 144421.

[66] M. Merkel, M. Reginka, R. Huhnstock, A. Ehresmann, Polycrystalline exchange-biased bilayers: Magnetically effective versus structural antiferromagnetic grain volume distribution, Phys. Rev. B 106 (2022) 014403.

[67] K. O'Grady, L.E. Fernandez-Outon, G. Vallejo-Fernandez, A new paradigm for exchange bias in polycrystalline thin films, J. Magn. Magn. Mater. 322 (2010) 883–899.

[68] C.R. Pike, First-order reversal-curve diagrams and reversible magnetization, Phys. Rev. B 68 (2003) 104424.

[69] S. Ruta, O. Hovorka, P.-W. Huang, K. Wang, G. Ju, R. Chantrell, First order reversal curves and intrinsic parameter determination for magnetic materials; Limitations of hysteron-based approaches in correlated systems, Sci. Rep. 7 (2017) 45218.

[70] K. Miyazawa, S. Okamoto, T. Yomogita, N. Kikuchi, O. Kitakami, K. Toyoki, D. Billington, Y. Kotani, T. Nakamura, T. Sasaki, T. Ohkubo, K. Hono, First-Order Reversal Curve analysis of a Nd-Fe-B sintered magnet with soft x-ray magnetic circular dichroism microscopy, Acta Mater. 162 (2019) 1–9.

[71] A.P. Roberts, T.P. Almeida, N.S. Church, R.J. Harrison, D. Heslop, Y. Li, J. Li, A.R. Muxworthy, W. Williams, X. Zhao, Resolving the origin of pseudo-single domain magnetic behavior, J. Geophys. Res. Sol. Ea. 122 (2017) 9534–9558.

[72] J. Xu, K. Zhu, W. Li, X. Wang, Z. Yang, Y. Hou, S. Gao, First-order-reversal-curve analysis of rare earth permanent magnet nanostructures: Insight into the coercivity enhancement mechanism through regulating the Nd-rich phase, Inorg. Chem. Front. 8 (2021) 1975–1982.